Published in final edited form as:
Nat Struct Mol Biol. 2019 May ; 26(5): 350–360. doi:10.1038/s41594-019-0214-1.

A symmetric toggle switch explains the onset of random X inactivation in different mammals

Verena Mutzel[1], **Ikuhiro Okamoto**[2,3], **Ilona Dunkel**[4], **Mitinori Saitou**[5,6,7], **Luca Giorgetti**[8], **Edith Heard**[9,10], and **Edda G. Schulz**[11,*]

[1]Otto Warburg Laboratories, Max Planck Institute for Molecular Genetics, Berlin, Germany [2]Department of Anatomy and Cell Biology, Graduate School of Medicine, Kyoto University, Kyoto 606-8501, Japan [3]Japan Science and Technology (JST), Exploratory Research for Advanced Technology (ERATO), Kyoto 606-8501, Japan [4]Otto Warburg Laboratories, Max Planck Institute for Molecular Genetics, Berlin, Germany [5]Institute for the Advanced Study of Human Biology (ASHBi), Kyoto University, Kyoto, 606-8501, Japan [6]Department of Anatomy and Cell Biology, Graduate School of Medicine, Kyoto University, Kyoto 606-8501, Japan [7]Center for iPS Cell Research and Application (CiRA), Kyoto University, Kyoto 606-8507, Japan [8]Friedrich Miescher Institute for Biomedical Research, Basel, Switzerland [9]Institut Curie, PSL Research University, CNRS UMR3215, INSERM U934, Paris, France [10]European Molecular Biology Laboratory (EMBL), Directors' research unit, Heidelberg, Germany [11]Otto Warburg Laboratories, Max Planck Institute for Molecular Genetics, Berlin, Germany

Abstract

Gene-regulatory networks control establishment and maintenance of alternative gene expression states during development. A particular challenge is the acquisition of opposing states by two copies of the same gene, as it is the case in mammals for *Xist* at the onset of random X-chromosome inactivation (XCI). The regulatory principles that lead to stable mono-allelic expression of *Xist* remain unknown. Here, we uncovered the minimal *Xist* regulatory network, by combining mathematical modeling and experimental validation of central model predictions. We identified a symmetric toggle switch as the basis for random mono-allelic *Xist* up-regulation, which reproduces data from several mutant, aneuploid and polyploid murine cell lines with various *Xist* expression patterns. Moreover, this toggle switch explains the diversity of strategies employed

*Corresponding Author: edda.schulz@molgen.mpg.de.

Code Availability

All code and simulations used in this study are available at https://github.com/verenamutzel/XCI_model under the MIT license.

Data Availability

Source data for figure 3c, 3d, 4b, 4c, 4f, 4g, 4i, 5d, 6c-f, S1, S3a, S3b, S3d are available with the paper online. Data, code and simulations used in this study are available at https://github.com/verenamutzel/XCI_model under the MIT license. All other data and the cell line TX1072dT generated for this study is available upon request.

Author contributions

Conceptualization, E.G.S., E.H. and I.O.; Software, V.M. and E.G.S.; Investigation, V.M., I.O., I.D., L.G., E.G.S.; Writing, E.G.S. and V.M. with input from E.H. and L.G; Supervision, E.G.S., E.H., M.S.; Funding Acquisition, E.G.S., E.H., L.G., I.O., M.S.

Competing Interests

The authors declare no competing interests.

Europe PMC Funders Author Manuscripts

by different species at the onset of XCI. In addition to providing a unifying conceptual framework to explore X-chromosome inactivation across mammals, our study sets the stage for identifying the molecular mechanisms required to initiate random XCI.

Introduction

During developmental cell fate decisions, cells must choose and subsequently maintain alternative transcriptional states. Such a decision-making process occurs at the onset of random X-chromosome inactivation (XCI), where 50% of cells in female embryos will silence the maternal (Xm) and 50% the paternal X chromosome (Xp). XCI is initiated during early embryogenesis by mono-allelic up-regulation of the long non-coding RNA (lncRNA) *Xist* from either the Xp or the Xm, which then induces chromosome-wide gene silencing *in cis*. *Xist* recruits repressive chromatin modifications including H3K27me3 to the inactive X, eventually resulting in complete heterochromatinization of the entire chromosome. In this way mammals ensure dosage compensation for X-linked genes between the sexes1.

While all eutherian mammals use *Xist* to control XCI, they appear to regulate it in different ways2. Human and rabbit embryos initially express *Xist* from both X chromosomes3, while mice are thought to exhibit strictly mono-allelic expression4,5. In rabbits the bi-allelic phase is very transient, but in human embryos it extends over several days, yet without inducing complete gene silencing3,6. Also some *Xist* regulators appear to be poorly conserved across species2. *Tsix*, *Xist's* repressive antisense transcription unit, regulates *Xist* in mice, but might not be functional in other mammals2,7,8, while another lncRNA, *XACT* antagonizes *Xist* in humans9. Therefore, different species have been suggested to employ diverse strategies to establish XCI during embryogenesis2.

To establish the female-specific mono-allelic expression pattern of *Xist*, a cell must (i) assess the number of X chromosomes, (ii) choose one for *Xist* up-regulation and (iii) stabilize two opposing states at the inactive X (Xi), which expresses *Xist*, and the active X (Xa) where *Xist* is silent1. The underlying regulatory network integrates information on X-chromosomal dosage, since cells with two or more X chromosomes, but not male or XO cells, up-regulate *Xist*10. Interestingly, cells with four X chromosomes inactivate three Xs when diploid (X tetrasomy), but only two when tetraploid, suggesting that also autosomal ploidy modulates the onset of XCI10,11.

Since the two *Xist* loci in a cell adopt opposing expression states, important regulatory events must occur in *cis*, on the allele level, indicating a role of X-linked regulators in mediating *cis*-regulation and transmitting X-dosage information. Indeed, several *cis*-acting lncRNA loci function as *Xist* repressors, like *Tsix* and potentially *Linx,* or as *Xist* activators, like *Ftx* and *Jpx*7,12–14. X-dosage sensing is thought to rely on a *trans*-acting X-linked *Xist* activator (XA), which by being present in a double dose in female cells, could confer female-specificity of XCI1. Silencing of XA upon mono-allelic *Xist* up-regulation would reduce its dose and thereby prevent *Xist* expression from the other allele through a *trans*-acting negative feedback loop15,16. Two *trans*-acting *Xist* activators have been proposed so far, the RNF12 (RLIM) protein, which is silenced by *Xist* and the lncRNA *Jpx*, which escapes XCI13,15,17.

Europe PMC Funders Author Manuscripts

While several regulators governing the initiation of XCI are known, their relative contributions and functional interplay, and the underlying regulatory principles remain poorly understood. To rigorously identify the interactions required to initiate random XCI we compare alternative network architectures through mathematical modeling and simulations and test model predictions experimentally. We show that the cooperation of a *cis*-acting repressor and a *trans*-acting activator is sufficient to ensure female-specific mono-allelic *Xist* up-regulation. They form an extended symmetric toggle switch, which can reproduce the diverse *Xist* expression patterns in aneuploid and polyploid cells, and in different species. Moreover, we show that in mice, the *cis*-acting repressor identified by our model comparison could be *Xist's* antisense transcript *Tsix*. Our systems biology approach has thus identified the regulatory principles governing the onset of XCI and provides a unifying framework of *Xist* regulation across species.

Results

A core network that can maintain mono-allelic *Xist* expression

To investigate the regulatory principles governing mono-allelic and female-specific *Xist* expression, we systematically screened alternative architectures of the underlying regulatory network. X-linked *Xist* regulators were classified in 8 categories depending on whether they activate (A) or repress (R) *Xist*, whether they act *in cis* (c) on the same chromosome or *in trans* (t) on both chromosomes and whether they are silenced during XCI or escape (e) (Fig. 1a). Using ordinary differential equations (ODE), we built 8 mathematical models of a cell with two Xs containing *Xist* and one regulator type (see supplementary note 1).

To understand which networks can maintain mono-allelic *Xist* expression, each model was simulated starting from an XaXi state, where *Xist* is only expressed from the Xi (simulation 1, Fig. 1b). Each simulation was performed for >10,000 randomly chosen parameter sets, combining different transcription rates and activation or repression strengths, to test whether a given network could in principle reproduce the experimental behavior. Only the network with a *cis*-acting *Xist* repressor (cXR) was able to maintain mono-allelic *Xist* expression (in 20% of parameter combinations, Fig. 1b). We further tested another 28 models, each combining two regulator types instead of one. Again, only the 7 cXR-containing models could stabilize mono-allelic expression making cXR the only factor strictly required to maintain the XaXi state (see supplementary note 1).

Next we tested, which network could also prevent *Xist* up-regulation from the single X in male (simulations 2+4) and from both Xs in female cells (simulation 3), by initiating the simulations from an Xa, XiXi or Xi state, respectively (Fig. 1c). We tested all 8 models that maintained the mono-allelic state in simulation 1, which contained cXR either alone or combined with another regulator type. While all tested networks maintained the Xa state in simulation 2, a *trans*-acting *Xist* activator (tXA) was required to prevent erroneous *Xist* expression in simulations 3 and 4. Female-specificity of *Xist* up-regulation does not require tXA to be subject to XCI (simulation 4); however to prevent bi-allelic expression tXA must be silenced (simulation 3). A comprehensive screening of 36 alternative network architectures thus identified a single minimal network (cXR-tXA) that can ensure the correct

Xist expression pattern (Fig. 2a). Although the *trans*-activator hypothesis has been previously proposed15 we show that, in addition correct XCI requires a *cis*-acting repressor.

The cXR-tXA model explains *Xist* patterns in diploid, polyploid and polysomic cells

We then asked whether the identified network could also recapitulate the initial establishment of a mono-allelic state (Fig. 2a+b). The XaXa-to-XaXi transition, where Xist is randomly up-regulated from either the Xm or Xp, cannot be simulated in the deterministic ODE framework used above. We therefore developed a stochastic cXR-tXA model, which simulates individual cells and accounts for random fluctuations (see supplementary note 2). For a subset of parameter values the network could indeed simulate robust mono-allelic *Xist* up-regulation (example simulations in Fig. 2c+d, for detailed analysis see supplementary note 2) and even reproduce experimental measurements quantitatively (Fig. S1a).

To understand how the cXR-tXA model controls mono-allelic *Xist* up-regulation, we analyzed *Xist's* expression states at the allele (Fig. 2e, top) and at the cell level (Fig. 2e,bottom). In post-XCI cells (XaXi) when one tXA copy is silenced (tXA dose=1), each allele can maintain either low or high *Xist* expression (bistability), corresponding to the Xa and Xi, respectively (Fig. 2e, top). Before XCI (tXA dose=2) only the *Xist*-high state exists, resulting in female-specific *Xist* up-regulation (XaXa, Fig. 2e). Upon complete tXA silencing in the XiXi state *Xist* expression cannot be sustained because the *Xist*-high state becomes unstable (XiXi, Fig. 2e). Consequently, the mono-allelic states (XaXi and XiXa), but not the *Xist*-negative and bi-allelic states, are stable at the cell level (Fig. 2e, bottom). Allelic and cellular bistability require both regulators. Without cXR only a single allelic state remains (Fig. 2f), whereas in the absence of tXA additional global states appear, such that coordination of the two *Xist* loci is lost and both the XaXa and the XiXi states become stable (Fig. 2g). In conclusion, this bistable behavior is generated by mutual repression of *Xist* and cXR, which form a *cis*-acting double-negative (=positive) feedback loop. tXA, which mediates a second, *trans*-acting feedback ensures female-specific and mutually exclusive expression of the two *Xist* alleles.

For further validation, we tested whether the cXR-tXA model could reproduce the phenotype of X aneuploidies, which inactivate all Xs except one10. Nearly all parameter sets that can reproduce mono-allelic *Xist* up-regulation in diploid female cells correctly predict no *Xist* expression in male and XO cells and bi- and tri-allelic expression in X-chromosome trisomies and tetrasomies, respectively (Fig. 2h). While diploid (2n) cells with four Xs inactivate three of them, tetraploid (4n) cells that also have 4 Xs only inactivate two11. Similarly, X-trisomic diploid cells inactivate two Xs, while triploid cells (3n) are a mixture of cells with one and two Xi11,18. We simulated polyploidy in two ways, assuming either that autosomal factors would repress tXA or that an additional copy of the genome leads to a 50% increase in nuclear volume19, thus resulting in an effective tXA dilution (see supplementary note 2 for details). In both scenarios the effective tXA concentration would be similar in diploid and in tetraploid nuclei. The majority of parameter sets that can reproduce mono-allelic *Xist* up-regulation in diploid XX cells correctly predicted, a mixture of cells in the Xi and XiXi states in triploid and the XiXi state in tetraploid cells in both scenarios (Fig. 2i+j). Parameter sets that can reproduce mono-allelic *Xist* up-regulation in

diploid female cells thus correctly reproduce also the different XCI patterns in X tri- and tetrasomies and in tri- and tetraploidies.

The cXR-tXA model explains *Xist* patterns in different species

In the cXR-tXA model bi-allelic *Xist* up-regulation can be reversed through tXA silencing (Fig. 2e). This could be the mechanism that resolves transient bi-allelic expression during rabbit embryogenesis3. Interestingly, bi-allelic *Xist* expression has not been observed in mouse embryos, but can occur in differentiating mouse embryonic stem cells (mESCs) (e.g. Fig. S1a, dots)20. To test if initiation of random XCI is associated with bi-allelic *Xist* up-regulation also *in vivo*, we assessed the *Xist* expression pattern by RNA FISH (fluorescence in situ hybridization) in the E5.0 epiblast where random XCI is first initiated, and indeed observed 15-20% of cells with two *Xist* clouds (Fig. 3a-c). In agreement with a recent study21, we conclude that transient bi-allelic *Xist* expression also occurs during mouse development, but less frequently than in rabbits or humans.

Our cXR-tXA model can generate different degrees of transient bi-allelic expression, depending on the relative time scales of tXA silencing and *Xist* up-regulation (Fig. S2a). A single network architecture can thus reproduce experimental data from both mouse and rabbit embryos, just assuming different values for the reaction rates (Fig. 3d). In contrast to rabbits, bi-allelic *Xist* expression in human embryos persists over several days without inducing gene silencing (only dampening of gene expression)3,6. How bi-allelic expression is resolved is unknown because this happens only after implantation into the uterus. In the cXR-tXA model, reduced gene silencing would lead to bi-allelic *Xist* expression, if (1) cXR is not yet expressed (Fig. 3e+S2b left) or if (2) cXR would be partially silenced ("dampened", Fig. 3e+S2b right), while tXA completely resisted *Xist*-mediated silencing, assuming variable susceptibility to dampening across genes. The onset of complete silencing (together with cXR up-regulation in scenario 1) would then induce the transition to the mono-allelic state. In summary, the cXR-tXA model can reproduce the different degrees of transient bi-allelic expression observed across mammals.

Bi-allelic *Xist* up-regulation is reversible

To validate the model experimentally, we tested its prediction that accelerating *Xist* up-regulation on one allele (=increased time before switch-ON of the other allele) should reduce the extent of transient biallelic *Xist* expression (Fig. S2a). We used an mESC cell line (TX1072), which was derived from a cross between two polymorphic mouse strains (C57BL6/J x Cast/EiJ), herein referred to as B6 and Cast, respectively, and carries a doxycycline-inducible promoter upstream of *Xist* on the B6 X chromosome (Fig. 4a, top), such that *Xist* up-regulation is accelerated by doxycycline treatment22. When cultured in 2i medium, the cells undergo random XCI upon differentiation frequently passing through a phase of bi-allelic *Xist* up-regulation20. As predicted (Fig. 4b), doxycycline addition one day before differentiation reduced bi-allelic *Xist* up-regulation from ~25% to <5% of cells (Fig. 4c). Accelerating *Xist* up-regulation can thus indeed modulate the extent of bi-allelic *Xist* expression.

Europe PMC Funders Author Manuscripts

Another prediction we aimed to test was that transient bi-allelic expression could be resolved to a mono-allelic state (see previous section). To this end, we artificially increased bi-allelic up-regulation and assessed the system's response. We deleted the *DXPas34* enhancer of *Tsix* from the Cast X chromosome in TX1072 mESCs (Fig. 4d), which results in preferential *Xist* up-regulation from that chromosome7. After 48h of differentiation *Xist* was induced by doxycycline also from the other allele (B6) (Fig. 4e), thus increasing the amount of bi-allelically expressing cells from ~10% to ~30% (Fig. 4f). Since *Xist* expression from the B6 chromosome is maintained by doxycycline, the cells are predicted to down-regulate *Xist* from the Cast chromosome to resolve the bi-allelic expression state (Fig. 4g top, light green). *Xist* expression was quantified in an allele-specific way through amplicon sequencing of single-nucleotide polymorphisms (SNPs) on cDNA. As predicted, *Xist* from the Cast chromosome was significantly down-regulated 48h after doxycycline treatment compared to the untreated control (Fig. 4g, bottom, light green).

To distinguish whether *Xist* up-regulation had indeed been reversed or whether silencing of both Xs had only lead to cell death, we performed two additional experiments. To assess viability, we quantified EdU incorporation during replication and found only slightly less EdU-positive cells in bi-allelic compared to mono-allelic cells after 24h of doxycycline treatment (88% vs 94%, Fig. S3c+d). Therefore, cell death only plays a minor role in the transition from the bi-allelic to the mono-allelic state. We also performed Immuno-RNA FISH for *Xist* and H3K27me3, which is recruited to the chromosome following *Xist* RNA coating1. 48h after doxycycline treatment we indeed identified chromosomes that had ceased to express *Xist*, but were still enriched for H3K27me3 (as this mark is lost more slowly from the X chromatin), and named these Xa* (scheme in Fig. 4e, example image Fig. 4h). Cells that had reverted from a bi-allelic to a mono-allelic state (Xa*Xi) were rarely observed after 4 days of differentiation without doxycycline (<5%), but constituted >10% of cells upon bi-allelic *Xist* induction (Fig. 4i). In conclusion, bi-allelic *Xist* expression can indeed be resolved by down-regulation of one *Xist* allele.

A mechanistic cXR-tXA model of murine *Xist* regulation

The identification of the regulator classes required for mono-allelic *Xist* up-regulation paves the way to uncovering the molecular identity of cXR and tXA. For the tXA factor no candidate with all required characteristics has been identified (see discussion for details). Among known cXRs, *Xist's* repressive antisense transcript *Tsix* is a well characterized *cis* repressor and has previously been suggested to function as a switch to establish mono-allelic *Xist* expression23. Mutual inhibition between *Xist* and *Tsix* could thus form the *cis*-acting double negative feedback loop we have predicted to generate bistability24. To test whether antisense transcription-mediated repression could generate bistability *in cis*, we developed a mechanistic model of the *Xist-Tsix* locus, describing transcriptional initiation, RNA-Pol II elongation and RNA degradation of this antisense gene pair (Fig. 5a, for details see supplementary note 3). The model assumes three mechanisms for mutual repression of *Xist* and *Tsix*: (1) *Xist* RNA-dependent silencing of the *Tsix* promoter, (2) *Tsix*-transcription dependent repression of the *Xist* promoter and (3) transcriptional interference25 (TI), occurring when Pol II complexes transcribing opposite strands meet, as modeled in several previous studies26,27. Since two Pol II complexes probably cannot bypass each other28, we

assumed that one complex will be removed from the locus. Through a multi-step simulation process we indeed identified parameter sets that reproduced random mono-allelic *Xist* up-regulation (example in Fig. 5b+c). This specific behavior is expected to occur only in a precise parameter regime and is therefore observed for a small fraction (~1%) of all tested parameter sets for such a complex model (7 parameters). To understand which inhibitory mechanisms were actually required, we tested 6 reductions of the full model ([1,2,3]). While two of the reduced models ([1,2], [1,3]) were able to maintain the XaXi state, only one of them [1,3], which retained *Xist*-dependent silencing and TI could reproduce mono-allelic *Xist* up-regulation (Fig. 5d). We named the [1,3] model the "antisense model" and used it for all further simulations. Interestingly, the reduced model [1,2], which lacked TI, could maintain, but not establish the XaXi state (cp. Fig. 5d top vs bottom), because the transition between the regime of stable XaXi maintenance and *Xist* up-regulation was too gradual (Fig. S4). A two-fold change in tXA levels did thus not allow a robust transition between the regimes, suggesting that TI might play an important role at the *Xist-Tsix* locus.

Transcriptional interference at the *Xist-Tsix* locus

To validate the existence of TI at the *Xist-Tsix* locus experimentally, we assessed whether forced *Xist* transcription would interfere with *Tsix* elongation. We used several mESC lines carrying the TX allele, where the endogenous *Xist* gene can be controlled by doxycycline (Fig. 6a), thus uncoupling *Xist* regulation from *Tsix* activity. Upon *Xist* induction in female TX1072 cells and an XO subclone of that line22 we quantified *Tsix* RNA transcribed from the TX allele by allele-specific analysis through pyrosequencing, and by qPCR, respectively (primer positions in Fig. 6b). In both cell lines, *Tsix* upstream of the overlapping region (5') was barely affected by *Xist* induction (Fig. 6c, dark blue), while quantification downstream of *Xist* (3') revealed a reduction by ~50% after 8h of doxycycline treatment (light blue). Also spliced *Tsix* was strongly reduced, since the splice acceptor site is close to the 3' end (Fig. 6c, purple). These results suggest that *Xist* induction indeed interferes with *Tsix* elongation.

To further validate TI at the *Xist-Tsix* locus, we measured nascent transcription by quantitative microscopy at the single cell level through RNA FISH with intronic oligonucleotide-based probes in a male TX mESC line (TXY)29. For *Tsix* we designed two different probes to detect transcription upstream of *Xist* (5') and within the overlapping region (3') (Fig. 6b). As expected, transcription of *Xist* and *Tsix* was mutually exclusive in nearly all cells after one day of doxycycline treatment (Fig. 6d+e, left). To be able to observe TI independent of *Xist* RNA mediated silencing, we used the silencing deficient TXYΔA line carrying a deletion of the *Xist* A-repeat29. In this line, mutually exclusive detection of *Xist* and *Tsix* in the overlapping region was still observed, while the *Tsix*-5' signal was now largely unaffected by *Xist* (Fig. 6e, right). When comparing the signal intensity of the two *Tsix* probes at *Xist* transcribing (*Xist*+) and not transcribing (*Xist*-) alleles, both *Tsix* signals were strongly reduced on the *Xist*+ alleles in the TXY line, likely due to *Xist*-RNA mediated silencing of *Tsix*. In TXYΔA cells the *Tsix*-5' region was unaffected by *Xist*, but the 3' position was strongly reduced, albeit to a lesser extent than in TXY cells (Fig. 6f). Although wildtype *Xis*t induces an even more complete repression, TI clearly perturbs transcriptional

elongation at the *Xist*-*Tsix* locus, thus validating a central assumption of the antisense model.

Xist and *Tsix* mutant phenotypes

To further validate the antisense model, we simulated known *Xist* and *Tsix* mutant phenotypes. For 100 parameter sets that could reproduce mono-allelic *Xist* up-regulation four genotypes were simulated: wildtype, $Tsix^{+/-}$, $Tsix^{-/-}$, $Xist^{+/-}$ (Fig. 7a-d). In our simulations, XCI in wildtype cells is random, such that 50% of cells will express *Xist* from one or the other X (Fig. 7a, bottom). In agreement with experimental observations7,30 heterozygous *Tsix* and *Xist* mutants undergo non-random XCI, where the mutant and wildtype Xs are silenced in $Tsix^{+/-}$ and $Xist^{+/-}$ cells, respectively (Fig. 7b+d, bottom). For homozygous *Tsix* mutants, 'chaotic' XCI has been described with a mixture of cells inactivating one or two X chromosomes31. In our simulations we observe *Xist* oscillations in this mutant, where bi-allelic *Xist* up-regulation results in complete tXA silencing, and subsequent *Xist* down-regulation, followed by another round of bi-allelic up-regulation (Fig. 7c, top). In agreement with the experimental phenotype, these simulations show a high frequency of bi-allelic *Xist* expression (Fig. 7c, bottom). We also analyzed the kinetics of *Xist* up-regulation, because XCI has been found to be accelerated in $Tsix^{+/-}$ cells, but slowed down in $Xist^{+/-}$ mESCs16. We calculated the half time of *Xist* up-regulation ($T_{1/2}$) where 50% of cells would have turned on *Xist* (example in Fig. 7e) and compared this value between mutant and wildtype simulations. For all parameter sets tested, a *Tsix* mutation indeed reduced, and an *Xist* mutation increased the half time of *Xist* up-regulation (Fig. 7f). These results support antisense-mediated repression of *Tsix* as a promising candidate mechanism for the predicted bi-stable feedback loop in mice.

Discussion

Through screening 36 alternative network architectures, we have identified a core network that can recapitulate random mono-allelic and female-specific *Xist* up-regulation. This network, consisting of a *trans*-acting activator and a *cis*-acting repressor, resembles an "extended toggle-switch", which is thought to govern many cell fate decisions through generating mutual exclusive expression of antagonizing lineage specifying factors32. While two transcription factors such as PU.1 and Gata1 (driving myeloid and lymphoid differentiation, respectively) mutually repress each other in a classical toggle switch32, the two *Xist* alleles inhibit each other through silencing of the *trans*-activating tXA factor. However, this inhibition cannot be directional, since reduction of any *trans*-acting regulator affects both *Xist* loci. Our analysis shows that the establishment of two alternative states in such a symmetric network, requires a local positive feedback mediated by a *cis*-repressor cXR, to memorize the initial choice of the inactive X, at least until the two states are locked in by epigenetic mechanisms such as DNA methylation1. Since transcription factors that drive cell fate decisions often promote their own expression through similar positive feedback regulation, cells seem to employ similar regulatory principles to ensure mono-allelic *Xist* up-regulation, as in other unrelated molecular decision-making processes.

We have identified the simplest network that can explain the onset of random XCI. While its mechanistic implementation might be more complex, our generic network can nevertheless serve as a framework to uncover the molecular identity of key regulators. Our approach is thus highly complementary to previous studies that have identified and characterized individual *Xist* regulators13–15,33. All known X-linked regulators can be grouped according to the classification we have developed (Table 1). While not explicitly accounted for in our modeling framework, autosomal factors might modulate reaction rates in a differentiation-dependent manner (e.g. pluripotency factors34–36) or mediate the effects of X-linked regulators (e.g. Rex1 as a target of RNF1237). X-linked regulators outside the identified core network might confer additional robustness (e.g. *Jpx*) or mediate interactions within the core network (e.g. a tXA factor could target *Ftx*).

So far, two *trans*-acting activators of *Xist* have been proposed (Table 1), the E3 ubiquitin ligase RNF12, which targets the *Xist* repressor Rex1 (Zpf42) for degradation, and the lncRNA *Jpx*13,15,37,38. While *Jpx* escapes XCI, *Rnf12* is rapidly silenced by *Xist* and is thus thought to form the *trans*-acting negative feedback loop that we also identified through our network screening approach15. Although RNF12 overexpression can induce *Xist* ectopically in male cells, its deletion in females cannot prevent *Xist* up-regulation15,39–41. Thus RNF12 either acts in concert with other tXA regulators or a so far unidentified tXA factor mediates the *trans*-acting negative feedback.

The cXR factor is likely a lncRNA, since they frequently act *in cis*42. In mice, two such loci, *Tsix* and *Linx (Ppnx)* have been described12,33. Since transcription seems to be dispensable for the function of *Linx* (R. Galupa, E. Heard, personal communication), it is probably insensitive to *Xist*-mediated silencing and would thus not form a double negative feedback loop. *Tsix*, by contrast, exerts its repressive function by transcription through the *Xist* promoter, where it induces repressive histone modifications43,44. Using a mechanistic mathematical model we show that mutual repression of *Xist* and *Tsix* can generate a local switch. Through transcriptional interference, which we confirmed to occur experimentally, antisense transcription can generate the precise threshold required for reliable mono-allelic *Xist* up-regulation. While the function of *Tsix* in mice is well documented, its conservation in other mammals, such as humans has not been shown2. Human *TSIX* has so far neither been detected in embryonic stem cells nor in embryos. Its transcription has only been reported in rather undefined embryoid body derived cells, albeit truncated compared to mouse *Tsix* and co-expressed with *XIST* from the same allele8. However, since the establishment of random XCI has not yet been observed neither *in vivo* nor *in vitro*, it might still be accompanied by *TSIX* transcription45. Even with the reduced overlap between *XIST* and *TSIX* reported for the human locus, the TI-based switch assumed in our antisense model could in principle ensure mono-allelic *XIST* expression (Fig. S6). *TSIXs* functional conservation in humans therefore remains an open question.

Generally, the positive feedback loop predicted to generate bistability must not necessarily be mediated by mutual repression of *Xist* and a cXR. Also differential chromatin modifications can maintain alternative states, e.g. at imprinted loci or at the *flc* locus in Arabidopsis46–49. Positive feedback loops are for example formed through reciprocal

Europe PMC Funders Author Manuscripts

stimulation of CpG and H3K9 methylation or through mutual antagonism of polycomb repression and transcription-associated H3K36 methylation46,50.

While the precise implementation of the positive feedback might vary between different mammals, the basic network structure we have identified can recapitulate all expression patterns observed in mice, humans and rabbits. Depending on the relative time scales of *Xist* up-regulation and gene silencing, the same network can recapitulate both low and high levels of bi-allelic *Xist* up-regulation as observed in mice and rabbit embryos, respectively3–5. Through ectopic induction of bi-allelic *Xist* expression we show that this state is reversible during early differentiation. This likely also occurs in mouse embryos *in vivo*, where we observe ~20% bi-allelic *Xist* expression at the onset of random XCI, in agreement with another recent study21.

Human pre-implantation embryos seem to be special because *Xist's* silencing ability is reduced or even absent3,6, possibly because factors that mediate silencing are not expressed at these developmental stages. The network we have identified predicts extended bi-allelic *Xist* expression (as observed in human embryos3) to arise from reduced gene silencing if either (1) cXR was not yet expressed at this stage or (2) cXR was dampened, while tXA was insensitive to *XIST*, assuming variable sensitivity to dampening across genes. Establishment of *XIST's* silencing capacity (together with cXR up-regulation in scenario 1) would induce a transition to the mono-allelic state. In particular scenario 1 is intriguing since antisense transcription, which appears to function as cXR in mice, is not observed during human pre-implantation development, but could potentially be up-regulated when the transition to the mono-allelic state occurs. Although so far the onset of random XCI could not be recapitulated with human ESCs45, further refinement of the culture conditions will hopefully allow us to test whether indeed mono-allelic *XIST* expression is established once silencing sets in and whether this might be accompanied by antisense transcription. Taken together, our study reveals that the regulatory principles employed by different mammalian species might be less diverse than previously thought and that the different routes to the mono-allelic state could be attributed to quantitative differences in reaction rates rather than qualitative differences in the network architecture.

Methods

ODE simulations

ODE models were formulated by assuming a Hill type regulation of production rates and first-order degradation rates, in a way that the levels of all variables were scaled between 0 and 1. Interaction between two regulators was assumed to occur synergistically, such that their effects are multiplied. The equation systems were simulated in Matlab using the ode23tb integrator for 100h, and the final state was used to solve for the steady state using the function fsolve. Details are given in supplementary note 1.

Stochastic simulations of the cXR-tXA model

Reactions describing production and degradation reactions were formulated directly from the ODE model, with adding scaling factors that would determine the maximal number of

molecules that can be produced for a given variable. Moreover, each *Xist* molecule had to transition through a certain number of silencing intermediates (with rate $1h^{-1}$) before reaching a silencing-competent state. The silencing delay for cXR (sil_{cXR}) and tXA (sil_{cXR}) was then given by the number of required silencing intermediates and is equal to the mean silencing delay. The simulations were performed using the Gillespie algorithm52, implemented in Julia and executed on a computing cluster. To identify parameter sets that could reproduce the experimental data, a large number of randomly chosen parameter sets were simulated. Experimental data and simulations were modeled with a multinomial distribution and a maximum likelihood estimate (MLE) was used to identify the parameter set that best explained the data. For further details, see supplementary note 2.

Stochastic simulations of the antisense model

To simulate antisense transcription, RNA Pol II molecules were assumed to bind to the promoters of *Tsix* and *Xist* in a stochastic fashion and then moved deterministically along the respective gene, which had been divided into 100nt-long segments. For elongation and degradation rates experimental estimates from the literature were used53–55. When *Xist* RNA exceeds a threshold of 10 molecules, the *Tsix* promoter will switch to the OFF state with a certain delay. Transcription of a *Tsix* polymerase through the *Xist* promoter, induced a switch to the OFF state, that could revert back to the ON state with a constant rate. When two RNA Pol II molecules occupied the same DNA segment, one randomly chosen polymerase was removed from the gene. tXA produced per allele was scaled between 0 and 1 and was set to 0 with a certain delay after *Xist* had exceeded a threshold of 10 molecules. Simulations were conducted in MATLAB. The model was written in C++ and compiled into a MEX file that was called from the main MATLAB function. For parameter scanning a compiled Matlab script was executed in parallel on a computing cluster.

Cell lines

The female TX1072 cell line and its subclone TX1072 XO (clone A11) are F1 hybrid ESCs (CastxB6), which carry a doxycycline responsive promoter in front of the *Xist* gene on the B6 chromosome and an rtTA insertion in the Rosa26 locus (described in22). The TX1072dT line (clone 1C6) was generated by introducing a deletion of the Dxpas34 repeat in TX1072 cells on the Cast chromosome by co-transfecting Cas9 expression vectors p33056 expressing sgRNAs GTACATAATGACCCGATCTC and GAACTCACTATATCGCCAAAG. Clones with the deletion were identified by PCR (ES585: AGGCACACCACCCCAGTGGA, ES609: TCCAAACATGGCGGCAGAAGC) and the deleted allele was identified by Sanger sequencing of the PCR product using primer ES609 based on two SNPs at positions 100,645,601 (Cast: C) and 100,641,221 (Cast: G) (mm9). Male-inducible wild-type and ΔA *Xist* lines were a gift from A. Wutz (called *Xist*-tetOP and *Xist*-ΔSX-tetOP, respectively, in29). All cell lines were regularly confirmed to be mycoplasma-negative.

ES cell culture and differentiation

TX1072, TX1072XO and TX1072dT cells were grown on gelatin-coated flasks in serum-containing ES cell medium (DMEM (Sigma), 15% FBS (Gibco), 0.1mM β-mercaptoethanol, 1000 U/ml leukemia inhibitory factor (LIF, Millipore)), supplemented with 2i (3 μM Gsk3 inhibitor CT-99021, 1 μM MEK inhibitor PD0325901) for TX1072 and

TX1072 XO. Differentiation was induced by 2i/LIF withdrawal in DMEM supplemented with 10% FBS and 0.1mM β-mercaptoethanol at a density of $4*10^4$cells/cm^2 in Fibronectin (10 μg/ml) coated tissue culture plates. For ectopic *Xist* induction the medium was supplemented with 1 μg/ml Doxycycline. To induce *Xist* in undifferentiated cells, they were plated at a density of $1*10^5$cells/cm^2 two days before harvesting and treated with 1 μg/ml doxycycline at the appropriate time points. Male-inducible wild-type and ΔA *Xist* lines were plated at a density of $3*10^4$cells/cm^2 on mitomycin-C-inactivated mouse embryonic fibroblasts in ES cell media containing 15% FBS (Gibco), 0.1mM β-mercaptoethanol (Sigma), 1,000 U/ml LIF (Millipore) and treated for 24 h with 2 μg/ml doxycycline one day after plating.

Mice

All animal experiments were performed under the ethical guidelines for the Care and Use of Laboratory Animals (French ethical committee of animal experimentation: Institut Curie #118 and agreement C75-05-17 for the animal facility; Kyoto University). Embryos were obtained by natural mating between B6D2F1 (derived from C57BL/6J and DBA2 crosses) female and males. Noon of the day when vaginal plugs were detected was set as E0.5.

Conventional RNA FISH on ESCs

FISH on cells from tissue culture was performed as described previously57. Briefly, mESCs were dissociated using Accutase (Invitrogen) and adsorbed onto Poly-L-Lysine (Sigma) coated coverslips #1.5 (1mm) for 5 min. Cells were fixed with 3% paraformaldehyde in PBS for 10 min at room temperature and permeabilized for 5 min on ice in PBS containing 0.5%Triton X-100 and 2mM Vanadyl-ribonucleoside complex (New England Biolabs). Coverslips were preserved in 70% EtOH at -20°C. Prior to FISH, samples were dehydrated through an ethanol series (80%, 95%, 100% twice) and air-dried quickly. For detecting the X-linked transcript Huwe1 (to verify the presence of two X chromosomes), a BAC spanning the respective genomic region (RP24-157H12) was labeled by nick translation (Abbot) using dUTP-Atto550 (Jena Bioscience). Per coverslip, 60ng probe was ethanol precipitated with Cot1 repeats, resuspended in formamide, denatured (10min 75°C) and competed for 1h at 37°C. *Xist* was detected with a custom designed strand-specific probe that densely tiles all exons with ~75bp long oligo nucleotides end-labeled with the Alexa488 fluorophore (Roche). Both probes were co-hybridized in FISH hybrization buffer (50% Formamide, 20% Dextran sulfate, 2x SSC, 1μg/μl BSA, 10mM Vanadyl-ribonucleoside) over night. Washes were carried out at 42°C three times 7min in 50% formamide in 2X SSC at pH=7.2 and three times 5min in 2X SSC. 0.2mg/mL DAPI was used for counterstaining and mounting medium consisted in 90% glycerol, 0.1X PBS, 0.1% p-phenylenediamine at pH9 (Sigma). Images were acquired using a wide-field DeltaVision Core microscope (Applied Precision) or a widefield Z1 Observer (Zeiss) using a 100x objective.

Immunofluorescence combined with RNA FISH

For immunofluorescence staining cells were differentiated on Fibronectin coated cover slips (18mm Marienfeld) at a density of $2*10^4$cells/cm^2. Cells were fixed and permeabilized as described above and incubated with the H3K27me3 antibody (Active Motif #39155, 0.4ug/ml) in PBS for 1h at room temperature, then washed 3 times for 10 minutes with PBS,

followed by a 1h incubation with an Alexa-555 labelled Goat anti-rabbit antibody (Invitrogen A-21428, 0.8 ug/ml). After 3 washes, the cells were fixed again with 3% paraformaldehyde in PBS for 10 min at room temperature, followed by three short washes with PBS and two washes with SSC. Hybridization was then performed as described above. Details on the antibodies used are found in supplementary table S1.

EdU staining combined with RNA FISH

Cells were differentiated on Fibronectin coated cover slips (18mm Marienfeld) at a density of $2*10^4$cells/cm^2 and were treated with 7.5μM EdU (Component A from Click-iT EdU Imaging kit Invitrogen C10340) for 2h before harvesting. Cells were fixed and permeabilized as described above, except that fixation and permeabilization were carried out at room temperature for 15 and 20 minutes, respectively. EdU staining with Alexa Fluor 647 was performed according to the manufacturer's recommendations, followed by RNA FISH for Xist as described above.

Quantitative RNA FISH

Quantitative RNA FISH on *Xist* and *Tsix* was performed using Stellaris FISH probes (Biosearch Technologies). Probe details can be found in table S1. Cells were adsorbed and fixed as described above. Cells were prehybridized in wash buffer (2x SSC, 10% formamide) twice for 5 min, then hybridized with a solution that contained 125 nM of each FISH probe, 2X SSC, 10% formamide, 10% dextran sulfate overnight at 37 °C. Cells were washed twice with wash buffer for 30 min before counterstaining DNA with 0.2mg/ml DAPI in 1x PBS, and mounted on slides using the mounting medium described above. Z-stacks were acquired using a wide-field Z1 observer (Zeiss) microscope equipped with a 100x objective (voxel size 88x88x200 nm). Quantification of nascent RNA signals was performed as in58. Briefly, the fluorescence background of each z plane was generated by morphologically opening the image with a circular structuring element with a diameter of 5 pixels (440 nm), and subtracted from the original image. A region of interest (ROI) of constant volume (30x30x6 pixels = 2.6x2.6x1.2μm) was selected around each transcription site. To reduce residual high-frequency fluorescence background, the average pixel intensity was measured in a 3-voxel thick frame adjacent to the border of the ROI, and further subtracted. The integrated intensity of the fluorescent signal was then measured within the whole ROI. Integrated intensities of approximately 500 random nuclear background ROIs were used to define a threshold (mean + 5*s.d after removing top 1% as outliers) to classify transcribed versus non transcribed loci.

RNA FISH of epiblast cells from E5.0 embryos

For E5.0 mouse embryos, the embryos were dissected out from decidua and the Reichert's membrane was removed in a 6cm Petri dish containing PBS using sharpened forceps. Extra-embryonic ectoderm was separated by a fine glass needle. The epiblast/visceral endoderm were incubated in 0.25% Pancreatin (Sigma) / 0.5% Trypsin / Polyvinylpyrrolidone (PVP40; Sigma) at 4°C for 10min and transferred to a 3.5cm petri dish containing a large volume of 1%BSA/PBS. Epiblast and visceral endoderm were separated by pipetting with a mouth pipette whose internal diameter is slightly smaller than that of the epiblast. RNA FISH was carried out as described previously5, using a non strand-specific probe detecting *Xist* and

Europe PMC Funders Author Manuscripts

Tsix (p510). Embryos with an *Xist* cloud were identified as female. Images were acquired using a 200M Axiovert fluorescence microscope (Zeiss) equipped with an ApoTome to generate 3D optical sections. Sequential z-axis images were collected in 0.3 μm steps. Images were analyzed using ImageJ software (Fiji, NIH).

RNA extraction, reverse transcription, qPCR

For pyrosequencing and qPCR, cells were lysed by direct addition of 1 ml Trizol (Invitrogen). Then 200μl of Chloroform was added and after 15 min centrifugation (12,000xg, 4°C) the aqueous phase was mixed with 700 μl 70% ethanol and applied to a Silica column (Qiagen RNAeasy Mini kit). RNA was then purified according to the manufacturer's recommendations, including on-column DNAse digestion. For quantitative PCR (qPCR), 1ug RNA was reverse transcribed using Superscript III Reverse Transcriptase (Invitrogen). Expression levels were quantified using 2x SybRGreen Master Mix (Applied Biosystems) and a ViiA7 system (Applied biosystems) with ~8ng cDNA and the primers given in table S1. Expression levels were normalized to Rrm2 and Rplp0.

Allele-specific amplicon sequencing

RNA was extracted using the Direct-zol RNA MiniPrep kit (Zymo Research) and DNase digest was performed using Turbo DNA free kit (Ambion). The TruSeq Targeted RNA Expression assay (Illumina) was used according to the manufacturer’s recommendations and the samples were sequenced on a HiSeq2500. For the quantification of reference genes (Rrm2, Rplp0, Fbxo28, Exoc1) 50bp reads were aligned to the mouse reference genome (mm10) with allowing 2 mismatches using the STAR aligner59 and the reads covering each amplicon were counted with Bedtools multicov60. For allele-specific quantification reads were aligned to either the B6 (reference) or Cast genomes with no mismatches and reads covering the SNPs were counted with Bedtool multicov. Reads for 4 amplicons within *Xist* exons containing SNPs were normalized to the geometric mean of the reference genes. The fold change of the doxycycline treated sample relative to the corresponding control sample was then calculated for each *Xist* amplicon. Using a one-sample t-Test it was tested whether the mean log2 fold-change of the four amplicons was significantly different from 0 ($p<0.05$). Details on the amplicons are given in supplementary table S1.

Pyrosequencing

For allele-specific expression analysis of *Tsix*, pyrosequencing technology was used. Two different amplicons within *Tsix*, each containing a SNP were PCR-amplified from cDNA with biotinylated primers and sequenced using the Pyromark Q24 system (Qiagen). Primer sequences are given in supplementary table S1. The assay provides the fraction of *Tsix* transcript arising from the B6 chromosome at time t (Ft). To calculate the expression from the B6 chromosome at time t relative to the uninduced state at t=0h ($\frac{B6_t}{B6_0}$) the data was transformed as follows. Assuming that expression from the Castaneus chromosome (Cast) is

constant over time, $F_0 = \frac{B6_0}{B6_0 + Cast}$ and $F_t = \frac{B6_t}{B6_t + Cast}$ can be transformed into $\frac{B6_t}{B6_0} = \frac{F_t(1 - F_0)}{F_0(1 - F_t)}$.

Statistics

Statistical significance was evaluated through a two-sided one- or two-sampled t-test, as indicated in the figure legends.

Supplementary Material

Refer to Web version on PubMed Central for supplementary material.

Acknowledgements

We thank A. Wutz (ETH Zürich, Switzerland) for the TXY (Xist-tetOP) and TXYΔA (Xist-ΔSX-tetOP) mESC lines. We thank the staff of the MPIMG and PICTIBiSA@BDD imaging facilities for technical assistance, the MPIMG sequencing core facility of sequencing services and the MPIMG IT for support in using the computing cluster. We thank R. Galupa for valuable feedback on the manuscript. Funding: This work was funded by an HFSP long-term fellowship (LT000597/2010-L) to E.G.S., a Grant-in-Aid for Specially Promoted Research from JSPS (17H06098) to M.S., and by a JST-ERATO Grant (JPMJER1104) to M.S. and JST-ERATO to I.O. and M.S., JSPS KAKENHI Grant (25291076 and 18K06030) to I.O.. Reseach in E.G.S.'s lab is funded by the Max-Planck Research Group Leader program and and the German Ministry of Science and Education (BMBF) through the grant E:bio Module III - Xnet. V.M. is supported by the DFG (GRK1772: Computational Systems Biology). Research in L.G.'s lab is funded by ERC Starting grant (759366).

References

1. Augui S, Nora EP, Heard E. Regulation of X-chromosome inactivation by the X-inactivation centre. Nature Reviews Genetics. 2011; 12:429–442.
2. Sado T, Sakaguchi T. Species-specific differences in X chromosome inactivation in mammals. Reproduction. 2013; 146:R131–9. [PubMed: 23847260]
3. Okamoto I, et al. Eutherian mammals use diverse strategies to initiate X-chromosome inactivation during development. Nature. 2011; 472:370–374. [PubMed: 21471966]
4. Mak W, et al. Reactivation of the paternal X chromosome in early mouse embryos. Science. 2004; 303:666–669. [PubMed: 14752160]
5. Okamoto I, Otte AP, Allis CD, Reinberg D, Heard E. Epigenetic dynamics of imprinted X inactivation during early mouse development. Science. 2004; 303:644–649. [PubMed: 14671313]
6. Petropoulos S, et al. Single-Cell RNA-Seq Reveals Lineage and X Chromosome Dynamics in Human Preimplantation Embryos. Cell. 2016; 165:1012–1026. [PubMed: 27062923]
7. Lee JT, Lu N. Targeted mutagenesis of Tsix leads to nonrandom X inactivation. Cell. 1999; 99:47–57. [PubMed: 10520993]
8. Migeon BR, Lee CH, Chowdhury AK, Carpenter H. Species differences in TSIX/Tsix reveal the roles of these genes in X-chromosome inactivation. Am J Hum Genet. 2002; 71:286–293. [PubMed: 12023758]
9. Vallot C, et al. XACT Noncoding RNA Competes with XIST in the Control of X Chromosome Activity during Human Early Development. Cell Stem Cell. 2017; 20:102–111. [PubMed: 27989768]
10. Brown CJ, et al. The human XIST gene: analysis of a 17 kb inactive X-specific RNA that contains conserved repeats and is highly localized within the nucleus. Cell. 1992; 71:527–542. [PubMed: 1423611]

11. Monkhorst K, et al. The Probability to Initiate X Chromosome Inactivation Is Determined by the X to Autosomal Ratio and X Chromosome Specific Allelic Properties. PLoS ONE. 2009; 4:e5616. [PubMed: 19440388]
12. Nora EP, et al. Spatial partitioning of the regulatory landscape of the X-inactivation centre. Nature. 2012; 485:381–385. [PubMed: 22495304]
13. Tian, Di; Sun, S; Lee, JT. The Long Noncoding RNA, Jpx, Is a Molecular Switch for X Chromosome Inactivation. Cell. 2010; 143:390–403. [PubMed: 21029862]
14. Furlan G, et al. The Ftx Noncoding Locus Controls X Chromosome Inactivation Independently of Its RNA Products. Molecular Cell. 2018; 70:462–472.e8. [PubMed: 29706539]
15. Jonkers I, et al. RNF12 Is an X-Encoded Dose-Dependent Activator of X Chromosome Inactivation. Cell. 2009; 139:999–1011. [PubMed: 19945382]
16. Monkhorst K, Jonkers I, Rentmeester E, Grosveld F, Gribnau J. X Inactivation Counting and Choice Is a Stochastic Process: Evidence for Involvement of an X-Linked Activator. Cell. 2008; 132:410–421. [PubMed: 18267073]
17. Sun S, et al. Jpx RNA activates Xist by evicting CTCF. Cell. 2013; 153:1537–1551. [PubMed: 23791181]
18. Endo S, Takagi N, Sasaki M. The late-replicating X chromosome in digynous mouse triploid embryos. Developmental Genetics. 1982; 3:165–176.
19. Henery CC, Bard JB, Kaufman MH. Tetraploidy in mice, embryonic cell number, and the grain of the developmental map. Developmental Biology. 1992; 152:233–241. [PubMed: 1644218]
20. Guyochin A, et al. Live cell imaging of the nascent inactive X chromosome during the early differentiation process of naive ES cells towards epiblast stem cells. PLoS ONE. 2014; 9:e116109. [PubMed: 25546018]
21. Sousa EJ, et al. Exit from Naive Pluripotency Induces a Transient X Chromosome Inactivation-like State in Males. Cell Stem Cell. 2018; 22:919–928.e6. [PubMed: 29804891]
22. Schulz EG, et al. The Two Active X Chromosomes in Female ESCs Block Exit from the Pluripotent State by Modulating the ESC Signaling Network. Cell Stem Cell. 2014; 14:203–216. [PubMed: 24506884]
23. Willard HF, Carrel L. Making sense (and antisense) of the X inactivation center. Proc Natl Acad Sci USA. 2001; 98:10025–10027. [PubMed: 11526224]
24. Loos F, et al. Xist and Tsix Transcription Dynamics Is Regulated by the X-to-Autosome Ratio and Semistable Transcriptional States. Molecular and Cellular Biology. 2016; 36:2656–2667. [PubMed: 27528619]
25. Shearwin KE, Callen BP, Egan JB. Transcriptional interference--a crash course. Trends in Genetics. 2005; 21:339–345. [PubMed: 15922833]
26. Sneppen K, et al. A mathematical model for transcriptional interference by RNA polymerase traffic in Escherichia coli. J Mol Biol. 2005; 346:399–409. [PubMed: 15670592]
27. Nakanishi H, Mitarai N, Sneppen K. Dynamical analysis on gene activity in the presence of repressors and an interfering promoter. Biophys J. 2008; 95:4228–4240. [PubMed: 18658208]
28. Hobson DJ, Wei W, Steinmetz LM, Svejstrup JQ. RNA Polymerase II Collision Interrupts Convergent Transcription. Molecular Cell. 2012; doi: 10.1016/j.molcel.2012.08.027
29. Wutz A, Rasmussen TP, Jaenisch R. Chromosomal silencing and localization are mediated by different domains of Xist RNA. Nature Genetics. 2002; 30:167–174. [PubMed: 11780141]
30. Penny GD, Kay GF, Sheardown SA, Rastan S, Brockdorff N. Requirement for Xist in X chromosome inactivation. Nature. 1996; 379:131–137. [PubMed: 8538762]
31. Lee JT. Regulation of X-Chromosome Counting by Tsix and Xite Sequences. Science. 2005; 309:768–771. [PubMed: 16051795]
32. Zhou JX, Huang S. Understanding gene circuits at cell-fate branch points for rational cell reprogramming. Trends in Genetics. 2011; 27:55–62. [PubMed: 21146896]
33. Lee JT, Davidow LS, Warshawsky D. Tsix, a gene antisense to Xist at the X-inactivation centre. Nature Genetics. 1999; 21:400–404. [PubMed: 10192391]
34. Navarro P, et al. Molecular coupling of Xist regulation and pluripotency. Science. 2008; 321:1693–1695. [PubMed: 18802003]

35. Donohoe ME, Silva SS, Pinter SF, Xu N, Lee JT. The pluripotency factor Oct4 interacts with Ctcf and also controls X-chromosome pairing and counting. Nature. 2009; 460:128–132. [PubMed: 19536159]
36. Schulz EG, Heard E. Role and control of X chromosome dosage in mammalian development. Current Opinion in Genetics & Development. 2013; 23:109–115. [PubMed: 23465885]
37. Gontan C, et al. RNF12 initiates X-chromosome inactivation by targeting REX1 for degradation. Nature. 2012; 485:386–390. [PubMed: 22596162]
38. Gontan C, et al. REX1 is the critical target of RNF12 in imprinted X chromosome inactivation in mice. Nature Communications. 2018; 9
39. Barakat TS, et al. RNF12 Activates Xist and Is Essential for X Chromosome Inactivation. PLoS Genet. 2011; 7:e1002001. [PubMed: 21298085]
40. Wang F, et al. Rlim-Dependent and -Independent Pathways for X Chromosome Inactivation in Female ESCs. Cell Rep. 2017; 21:3691–3699. [PubMed: 29281819]
41. Shin J, et al. RLIM is dispensable for X-chromosome inactivation in the mouse embryonic epiblast. Nature. 2014; 511:86–89. [PubMed: 24870238]
42. Quinn JJ, Chang HY. Unique features of long non-coding RNA biogenesis and function. Nature Reviews Genetics. 2016; 17:47–62.
43. Navarro P, Page DR, Avner P, Rougeulle C. Tsix-mediated epigenetic switch of a CTCF-flanked region of the Xist promoter determines the Xist transcription program. Genes & Development. 2006; 20:2787–2792. [PubMed: 17043308]
44. Sado T, Hoki Y, Sasaki H. Tsix silences Xist through modification of chromatin structure. Developmental Cell. 2005; 9:159–165. [PubMed: 15992549]
45. Khan SA, Audergon PNCB, Payer B. X-chromosome activity in naive human pluripotent stem cells—are we there yet? Stem Cell Investigation. 2017; 4:54–54. [PubMed: 28725650]
46. Rose NR, Klose RJ. Understanding the relationship between DNA methylation and histone lysine methylation. Biochim Biophys Acta. 2014; 1839:1362–1372. [PubMed: 24560929]
47. Inoue A, Jiang L, Lu F, Suzuki T, Zhang Y. Maternal H3K27me3 controls DNA methylation-independent imprinting. Nature. 2017; 547:419–424. [PubMed: 28723896]
48. Angel A, Song J, Dean C, Howard M. A Polycomb-based switch underlying quantitative epigenetic memory. Nature. 2011; 476:105–108. [PubMed: 21785438]
49. Dodd IB, Micheelsen MA, Sneppen K, Thon G. Theoretical analysis of epigenetic cell memory by nucleosome modification. Cell. 2007; 129:813–822. [PubMed: 17512413]
50. Yang H, Howard M, Dean C. Antagonistic Roles for H3K36me3 and H3K27me3 in the Cold-Induced Epigenetic Switch at Arabidopsis FLC. Curr Biol. 2014; 24:1793–1797. [PubMed: 25065750]
51. Sakata Y, et al. Defects in dosage compensation impact global gene regulation in the mouse trophoblast. Development. 2017; 144:2784–2797. [PubMed: 28684628]
52. Gillespie DT. Exact stochastic simulation of coupled chemical reactions. The Journal of Physical Chemistry. 1977; 81:2340–2361.
53. Jonkers I, Kwak H, Lis JT, Struhl K. Genome-wide dynamics of Pol II elongation and its interplay with promoter proximal pausing, chromatin, and exons. Elife. 2014; 3:e02407. [PubMed: 24843027]
54. Sun BK, Deaton AM, Lee JT. A Transient Heterochromatic State in Xist Preempts X Inactivation Choice without RNA Stabilization. Molecular Cell. 2006; 21:617–628. [PubMed: 16507360]
55. Yamada N, et al. Xist Exon 7 Contributes to the Stable Localization of Xist RNA on the Inactive X-Chromosome. PLoS Genet. 2015; 11:e1005430. [PubMed: 26244333]
56. Ran FA, et al. Genome engineering using the CRISPR-Cas9 system. Nat Protoc. 2013; 8:2281–2308. [PubMed: 24157548]
57. Chaumeil J, Augui S, Chow JC, Heard E. Combined immunofluorescence, RNA fluorescent in situ hybridization, and DNA fluorescent in situ hybridization to study chromatin changes, transcriptional activity, nuclear organization, and X-chromosome inactivation. Methods Mol Biol. 2008; 463:297–308. [PubMed: 18951174]

58. Giorgetti L, et al. Predictive polymer modeling reveals coupled fluctuations in chromosome conformation and transcription. Cell. 2014; 157:950–963. [PubMed: 24813616]

59. Dobin A, et al. STAR: ultrafast universal RNA-seq aligner. Bioinformatics. 2012; 29:15–21. [PubMed: 23104886]

60. Quinlan AR, Hall IM. BEDTools: a flexible suite of utilities for comparing genomic features. Bioinformatics. 2010; 26:841–842. [PubMed: 20110278]

60. Barakat TS, et al. The trans-activator RNF12 and cis-acting elements effectuate X chromosome inactivation independent of X-pairing. Mol. Cell,. 2014; 53:965–978. [PubMed: 24613346]

Europe PMC Funders Author Manuscripts

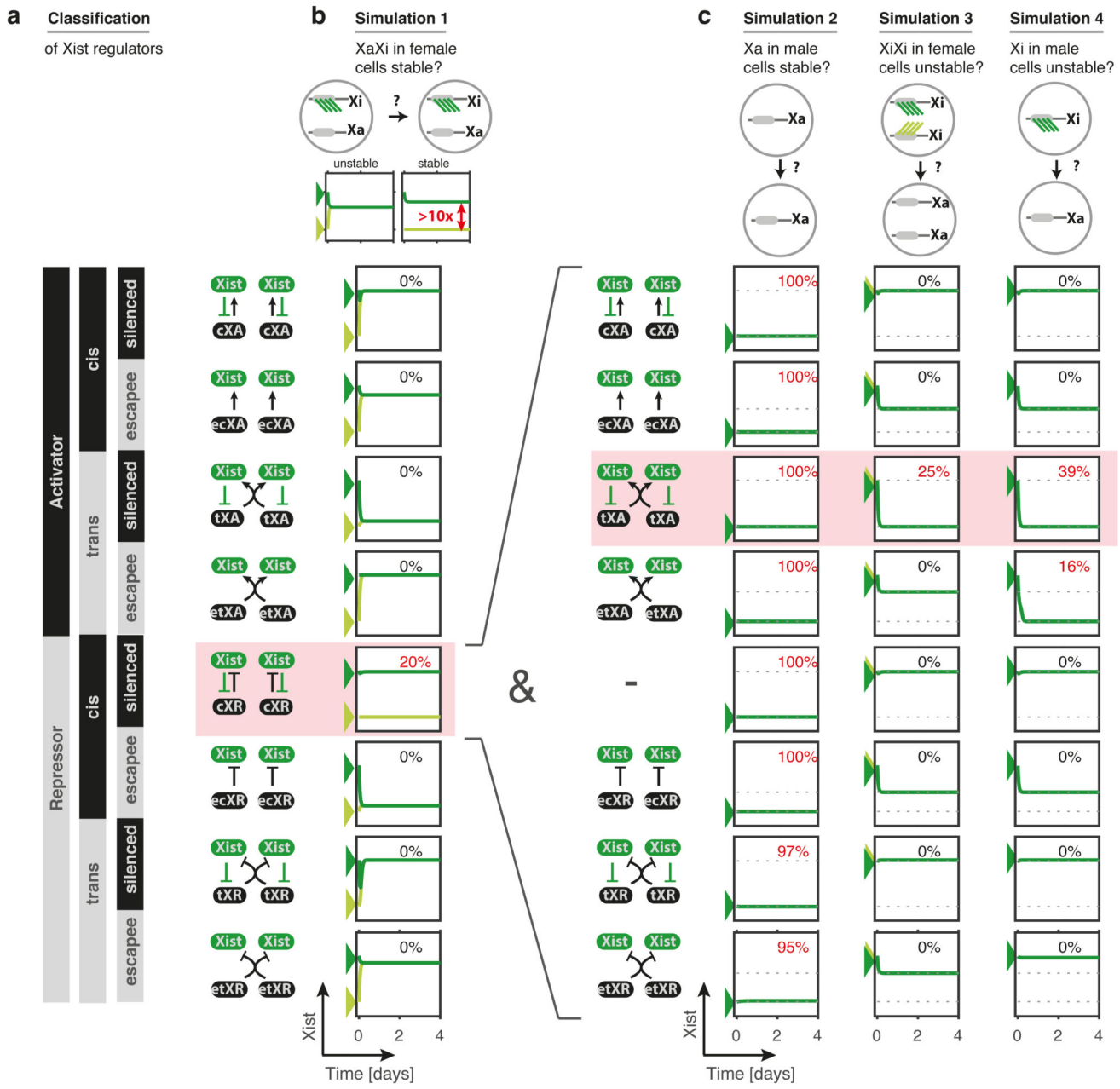

Figure 1. Comparison of alternative model structures

(a) Classification of X-linked *Xist* regulators, depending on whether they act as activators (XA) or repressors (XR), whether they act *in cis* (c) or *in trans* (t) and whether they are silenced during XCI or escape (e); schematic depiction of the networks formed by *Xist* and each regulator (right). **(b)** Each network was translated into a mathematical model (ODE), describing two X chromosomes, each carrying *Xist* and the respective regulator. Each model was simulated with >10,000 randomly chosen parameter sets initiating from an XaXi state (scheme, top), where *Xist* is expressed from one chromosome (dark green), and not from the other (light green). One example simulation is shown for each network and the percentage of

tested parameter sets, where the XaXi state was stably maintained is indicated (in red if >0%). **(c)** The *cis*-acting repressor (cXR), which could maintain the XaXi state in (b) was combined with all other regulator classes to build 7 more complex models. For all parameter sets that could maintain the XaXi state three additional simulations were performed to test whether the $Xist^{OFF}$ state (Xa) was maintained in male cells with a single X (simulation 2), whether bi-allelic *Xist* expression (XiXi) would be unstable in female cells (simulation 3) and whether *Xist* expression from the single X (Xi) in male cells would be unstable (simulation 4). One example simulation is shown for each model and the percentage of parameter sets that fulfill these criteria are shown. Dotted lines indicate the Xa and Xi state from the simulation in (b) and arrow heads denote the initial conditions. Shaded boxes indicate the model that can reproduce the experimental observations.

Europe PMC Funders Author Manuscripts

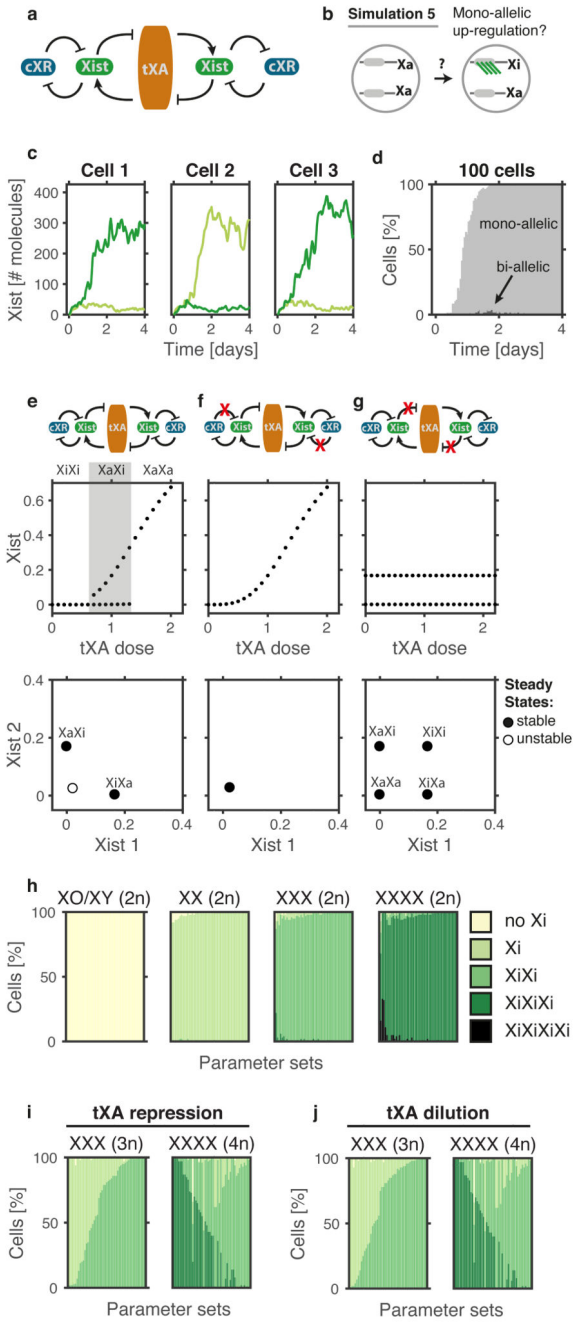

Figure 2. The cXR-tXA model can recapitulate *Xist* patterns in male, female, aneuploid and polyploid cell lines

(a-b) Schematic representation of the cXR-tXA model (a) and of the stochastic simulation (b) shown in (c-d), which initiates from the XaXa state found in undifferentiated cells. **(c-d)** Simulation of *Xist* up-regulation for one example parameter set, showing three individual cells (c) and a population of 100 cells (d). Light and dark green in (c) represent *Xist* levels expressed from the two X chromosomes, light and dark grey in (d) represent mono- and bi-allelic *Xist* expression, as indicated. **(e-g)** Steady state *Xist* levels simulated deterministically

(as in Fig. 1b) either for the full cXR-tXA model (e) or in the absence of either cXR-mediated repression (f) or tXA mediated activation (g). Allelic (top) and cellular (bottom) steady state levels are shown. Shaded area in (e) indicates the bistable regime for a single tXA dose corresponding to the mono-allelic XaXi state. Filled and open circles indicate stable and unstable steady states, respectively. In (g) tXA was assumed to be present at a constant single tXA dose (1x tXA). **(h)** Simulations of diploid cells with either one (left, male), two (middle left, female), three (middle right, X-trisomy) or four X chromosomes (right, X-tetrasomy). Stacked bar graphs show the classification of *Xist* patterns in simulations with 50 parameter sets that can generate robust mono-allelic *Xist* up-regulation in female diploid cells. **(i-j)** Stacked bar graphs show the classification of *Xist* patterns in simulations of triploid (left) and tetraploid cells (right) assuming that tXA is repressed by autosomal factors in a dose-dependent manner (i) or that tXA is diluted 1.5- and 2-fold in tri- and tetraploid cells, respectively, due to increased nuclear volume in polyploid cells (j). Details on the simulations are given in supplementary note 2.

Europe PMC Funders Author Manuscripts

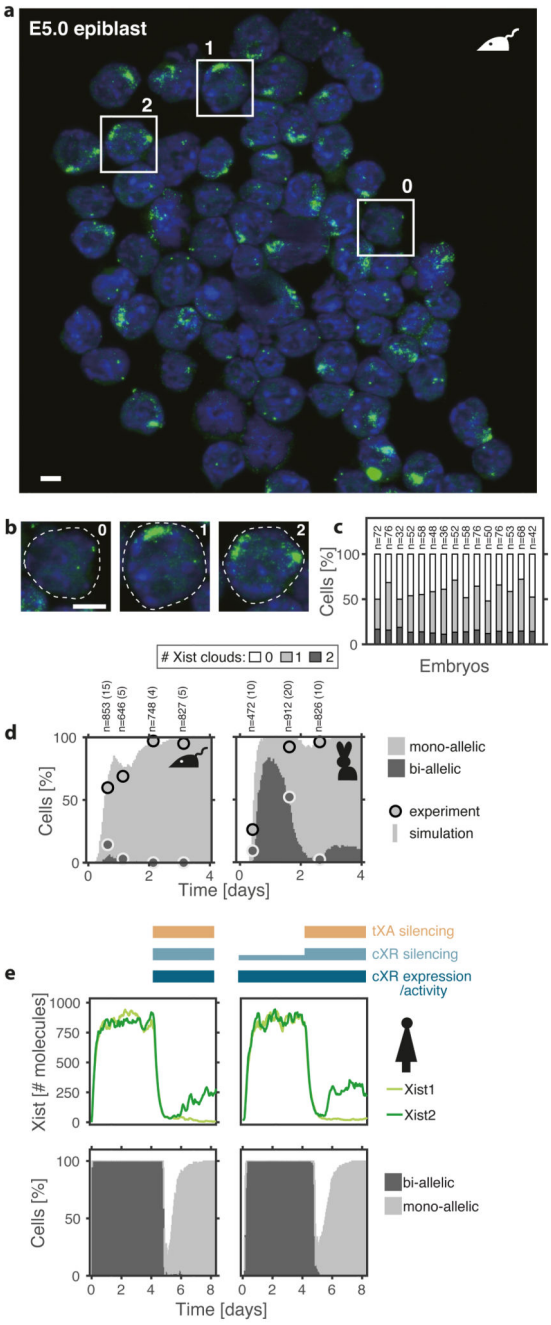

Figure 3. The cXR-tXA model reproduces transient bi-allelic expression in different species

(a-c) Non strand-specific RNA FISH (green) detecting both *Xist* and *Tsix* and nuclear staining (blue) of female mouse epiblast cells at E5.0 of embryogenesis. Scale bar 5μm. (b) Example cells with 0, 1 and 2 *Xist* clouds marked in (a) are enlarged, dashed white lines indicate the outlines of the nuclei. (c) The percentage of cells in each category is given across 15 female embryos, the number of cells counted is given above each bar. **(d)** Fraction of cells exhibiting mono-allelic (light grey) and bi-allelic *Xist* expression (dark grey) during early mouse (left) and rabbit development (right). Experimental data (circles) are shown

Europe PMC Funders Author Manuscripts

together with a simulation using the parameter set that best explains the data. The experimental data are taken from51,3 and (a-c). The total number of cells (n) counted for each time point is given on top, together with the number of embryos from which the data was pooled (in parentheses). **(e)** Simulation of bi-allelic expression upon reduced *Xist*-mediated silencing as observed in human embryos, assuming that in the first 4 days of the simulation either silencing (orange and light blue bars) and cXR expression (dark blue) is absent (left) or that cXR is silenced partially (light blue), while tXA (orange) is unaffected by *Xist* (right), as indicated. Simulations of an individual cell (top) and a population of 100 cells (bottom) for one example parameter set are shown. A summary of all parameter sets is given in supplementary figure S2b. Source data for panels c and d are available online.

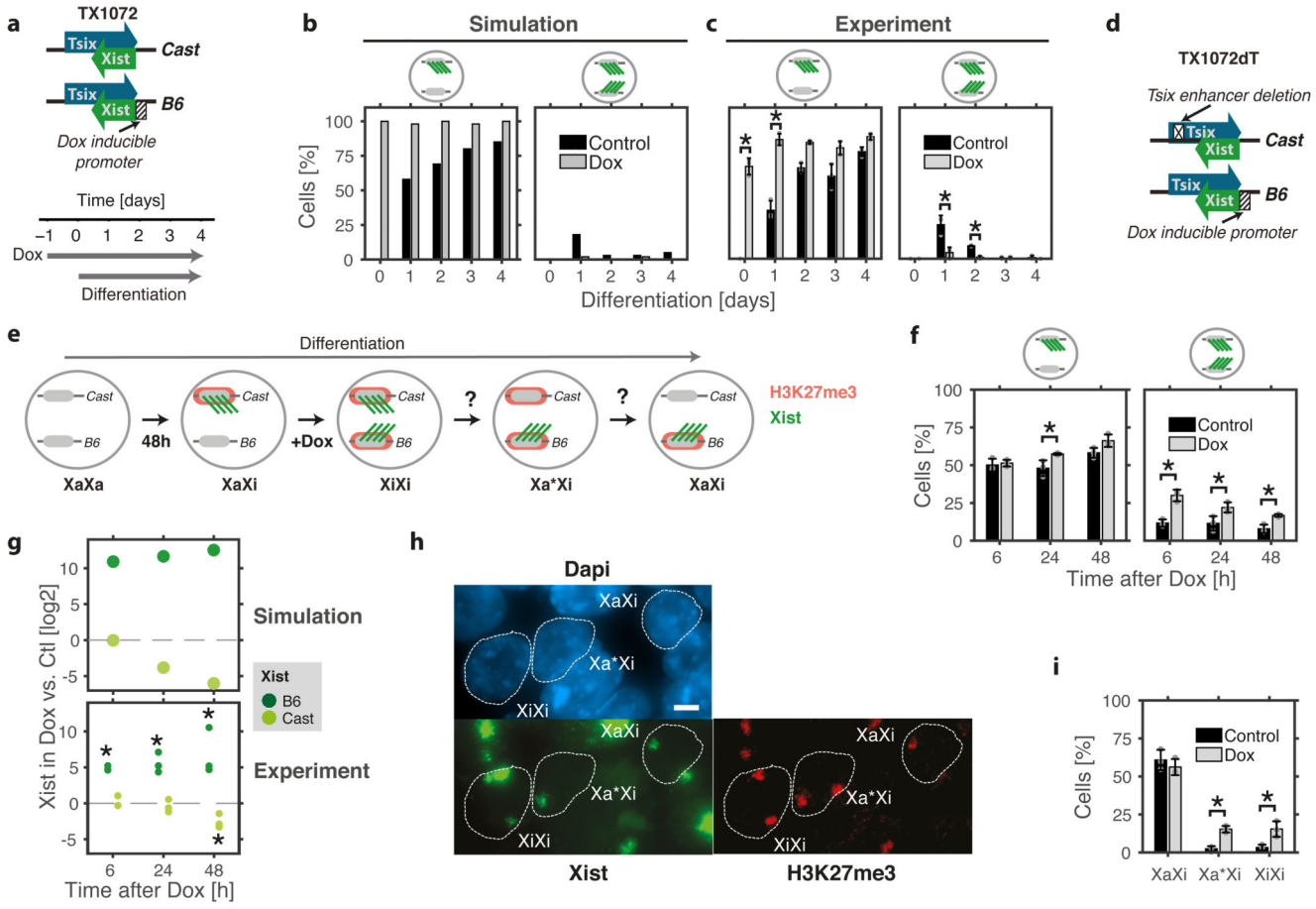

Figure 4. Bi-allelic *Xist* up-regulation is reversible

(a) Schematic representation of the cell line used (top) and treatment performed (bottom) in (b-c). (b-c) In a simulation (b) and in an experiment (c) cells were treated with doxycycline one day before differentiation and the percentage of cells showing mono-allelic (left) and bi-allelic *Xist* up-regulation (right) is shown. **(b)** The simulation for one example parameter set is shown; the results for all tested parameter sets can be found in Fig. S3a. **(c)** *Xist* patterns were assessed by RNA FISH. Mean and s.d. of n=3 independent experiments are shown (>80 cells/replicate, for details see source data). **(d-i)** Bi-allelic *Xist* up-regulation is artificially induced by treating TX1072dT cells (d) with doxycycline after 48h of differentiation. **(e)** The model predicts *Xist* down-regulation from the Cast chromosome, potentially with a transition through an Xa* state, where H3K27me3 (red) is still enriched, while *Xist* (green) has already been down-regulated. **(f)** *Xist* expression pattern at different time points after doxycycline addition as assessed by RNA FISH. Mean and s.d. of n=3 independent experiments are shown (>100 cells/replicate, for details see source data). **(g)** *Xist* expression levels from the B6 and Cast alleles at different time points after doxycycline treatment as predicted by the simulation (top) and measured experimentally by allele-specific amplicon sequencing (bottom). In the simulation one example parameter set is shown; results for all other tested parameter sets can be found in supplementary Fig. S3b. **(h-i)** Immunofluorescence followed by RNA FISH to detect *Xist* and H3K27me3 48h after

Europe PMC Funders Author Manuscripts

doxycycline induction. **(i)** Three states were quantified (XaXi, Xa*Xi, XiXi) as shown in the example image, scale bar indicates 5μm (h). Mean and s.d. of n=3 independent experiments are shown (>120 cells/replicate). *p<0.05 in two-sample (c,f,i) or one-sample (g) two-sided T-test. Source data for panels b, c, f, g, i are available online.

Europe PMC Funders Author Manuscripts

Europe PMC Funders Author Manuscripts

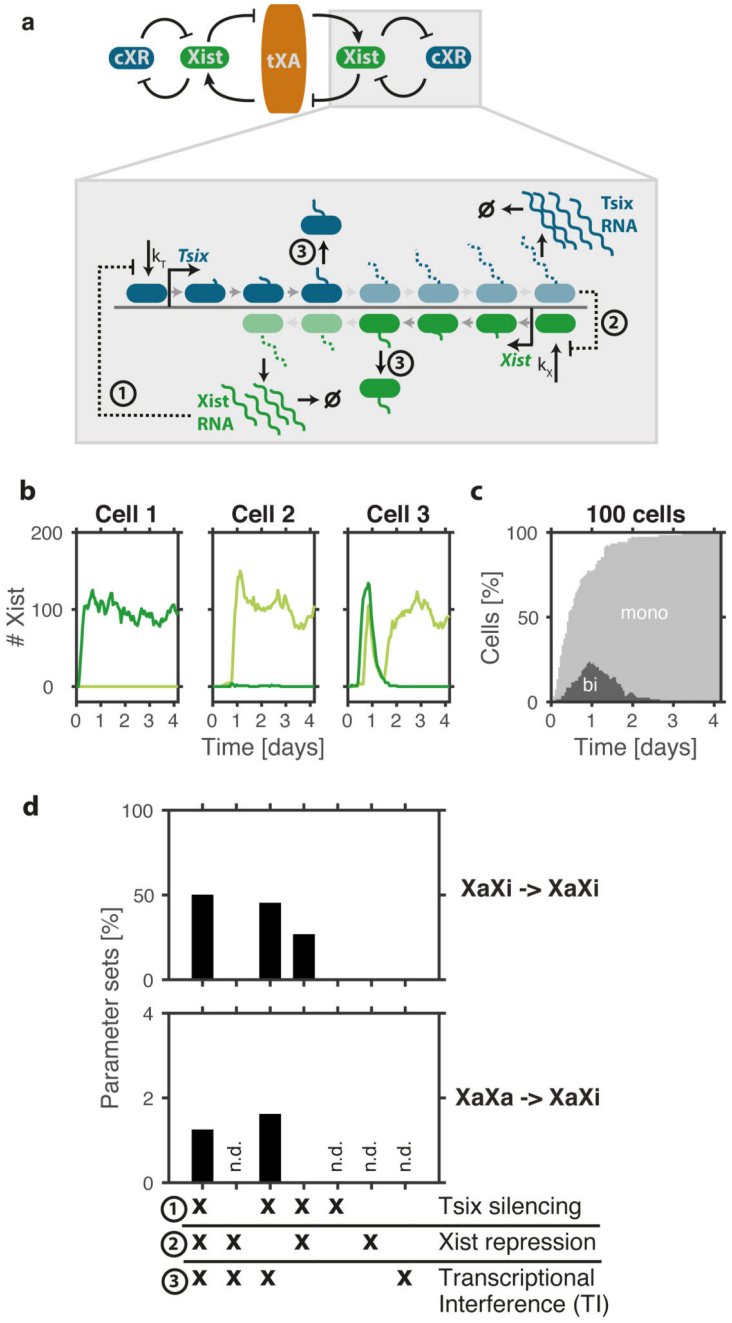

Figure 5. Predicted *cis*-acting feedback can be mediated by antisense transcription

(a) Schematic representation of the model were *Tsix* acts as the predicted *cis*-acting repressor: RNA Pol II complexes can bind to the *Tsix* (blue) and *Xist* (green) promoters and then move along the gene in a convergent fashion. Mutual repression occurs at three levels: (1) Silencing of the *Tsix* promoter by *Xist* RNA, (2) repression of the *Xist* promoter by antisense transcription and (3) random removal of one Pol II complex, if two antisense Pol II complexes occupy the same DNA element. Black dotted lines indicate interactions removed in the reduced models in (d). Lighter colors and dotted nascent RNA indicate potential

interruption of transcription through TI. **(b-c)** Stochastic simulation of *Xist* up-regulation for one example parameter set for the model shown in (a), showing three individual cells (b) and a population of 100 cells (c). Light and dark green in (b) represent *Xist* levels expressed from the two X chromosomes, light and dark grey in (c) represent mono- and bi-allelic *Xist* expression, as indicated. **(d)** Testing of model simplifications for the network in (a), where *Xist* and *Tsix* interact through one or two of the three repressive mechanisms as indicated. The percentage of parameter sets that can maintain the XaXi state (top) and that can initiate mono-allelic *Xist* up-regulation (bottom) in a stochastic simulation for each model are shown. Mono-allelic up-regulation was only tested for parameter sets that could maintain the XaXi state (others n.d.). Source data for panel d are available online.

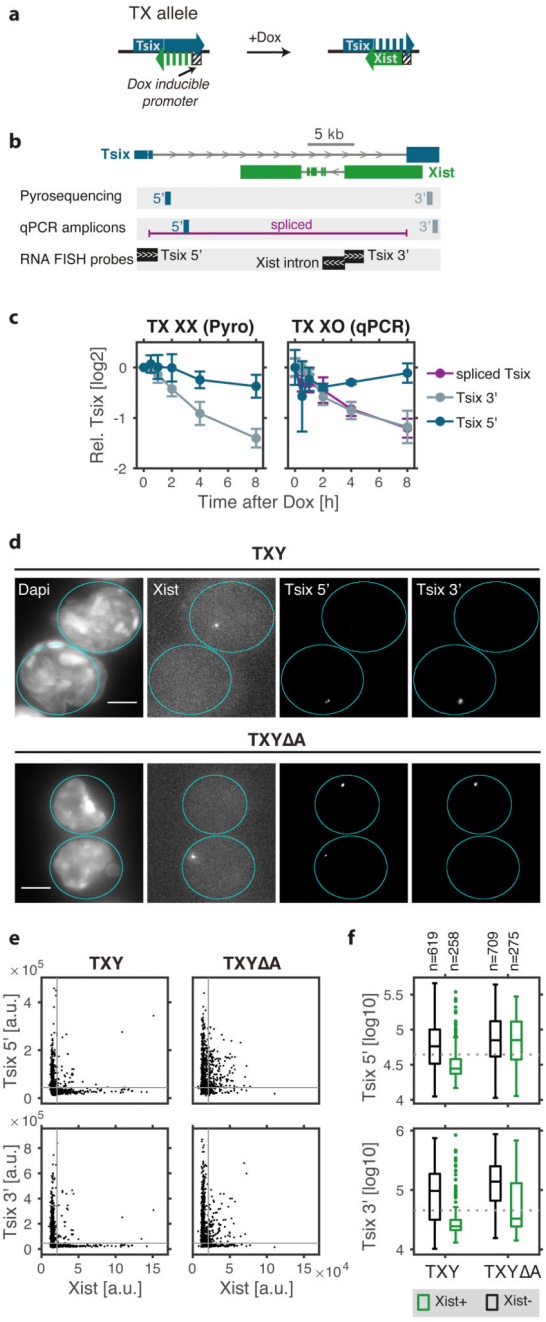

Figure 6. Transcriptional interferences at the *Xist-Tsix* locus

(a) The TX allele carries a doxycycline-inducible promoter driving the endogenous *Xist* gene and was used to investigate whether *Xist* transcription would interfere with *Tsix* elongation in (c-f). **(b)** Position of primers and probes used in (c-f). **(c)** TX1072 XX (left) and TX1072 XO ESCs (right) were treated with doxycycline for 8 h and *Tsix* transcription from the TX allele was assessed by pyrosequencing (XX) or qPCR (XO) at different positions within the *Tsix* gene. Mean and s.d. of n=3 independent experiments are shown. **(d-f)** TXY and TXYΔA ESCs were treated with doxycycline for 24 hours and nascent

transcription of *Xist* and *Tsix* (5' and 3') was assessed by RNA FISH (probe positions in b). Example images (d) and quantification (e) of n=877 (TXY) and n=984 cells (TXY ΔA) are shown, where each dot represents the measured signal intensities of a single allele. Scale bar 5μm. Grey lines indicate the detection threshold estimated from negative control regions. **(f)** Box plots of *Tsix* signal intensity at *Xist*+ (green) and *Xist*- alleles (black) in the two cell lines as indicated (center line, median; box limits, upper and lower quartiles; whiskers, most extreme data points not considered outliers; points, outliers). The data shown in (e-f) was pooled from 3 independent biological replicates (individual replicates are shown in Fig. S5). Source data for panels c, e and f are available online.

Europe PMC Funders Author Manuscripts

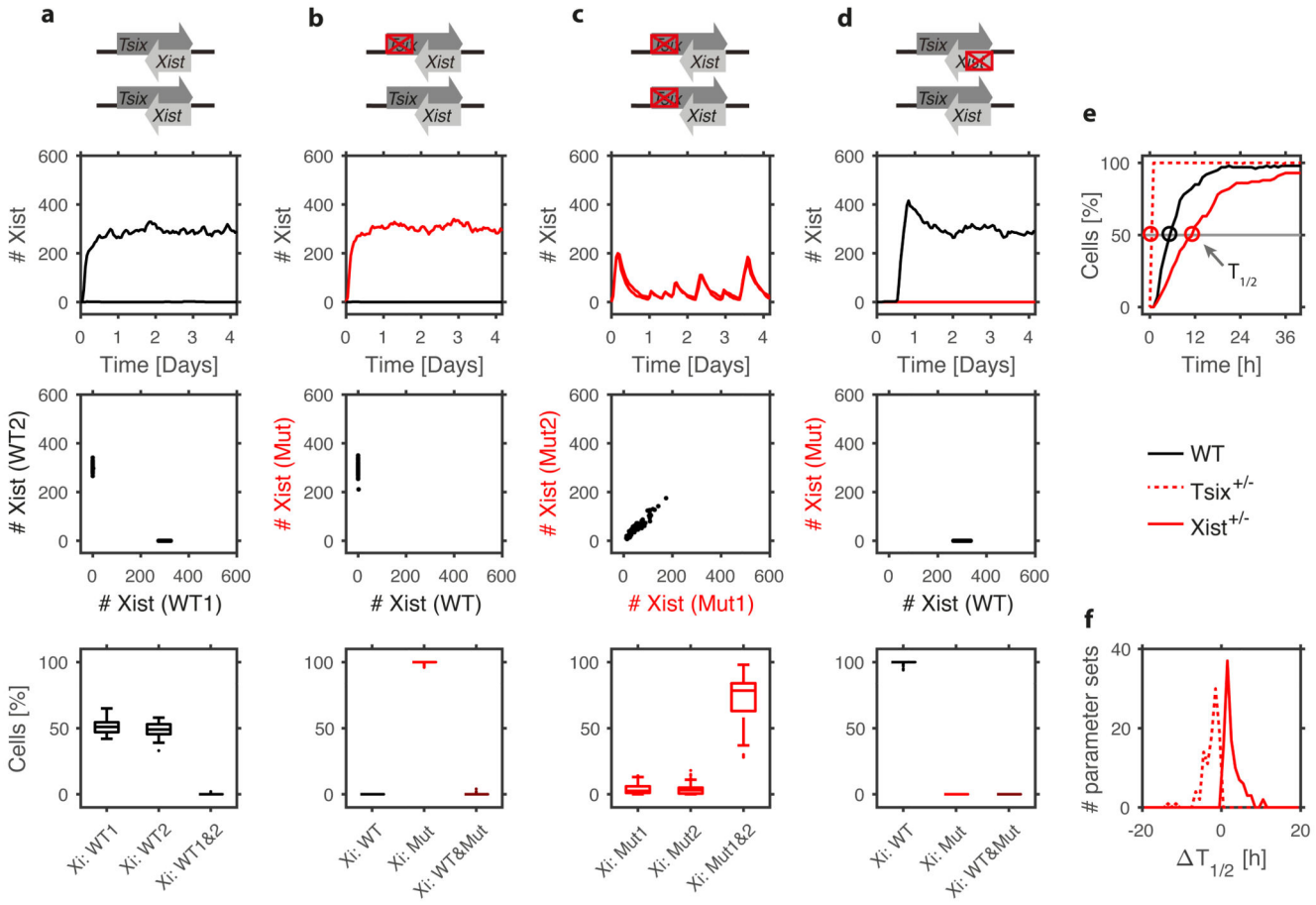

Figure 7. Simulating *Xist* and *Tsix* mutant cell lines

(a-d) Simulations of *Xist* and *Tsix* mutant cell lines as indicated on top. Representative simulation of *Xist* levels produced by the wildtype (WT, black) and mutant (Mut, red) chromosomes in a single cell (upper middle) and by 100 cells (lower middle). Boxplots (bottom) show the percentage of cells expressing *Xist* mono-allelically from wildtype or mutant X or bi-allelically for n=100 simulated parameter sets (center line, median; box limits, upper and lower quartiles; whiskers, most extreme data points not considered outliers; points, outliers). **(e-f)** *Xist* up-regulation is accelerated in $Tsix^{+/-}$ and delayed in $Xist^{+/-}$ cells. Representative simulation (e) and the distribution of the change of half time ($\Delta T_{1/2}$) in the mutant genotypes (f).

Europe PMC Funders Author Manuscripts

Europe PMC Funders Author Manuscripts

Table 1

X-linked Xist regulators

Regulator class	Putative members
cXA	-
ecXA	*Ftx*14, *Jpx*13,1761
tXA	RNF1215,37,41
etXA	*Jpx*13,17
cXR	*Tsix*7, *Linx*12
ecXR	-
tXR	-
etXR	-